Debonding Patch Detection in FRP-Strengthened Materials with Fiber-Optic Interferometer

Xu Ying *, *Wang Dexiang*, *Tang Tianyou*, *Lu Miaomiao*

Shenzhen Key Lab of Urban & Civil Engineering Disaster Prevention & Reduction, Harbin Institute of Technology Shenzhen Graduate School, Shenzhen 518055, P. R. China

(Received 30 September 2016; revised 8 May 2017; accepted 20 May 2017)

Abstract: The interfacial debonding in fiber-reinforced plastic(FRP) strengthened repair material will affect the bonding strength and lead to failure of the repair without warning. Unfortunately the interfacial damage is normally invisible and often in the form of a patch rather than a through-width crack. Therefore, a debonding patch detection technique based on fiber optic interferometry is proposed. A quasi-impulse loading is applied with a rubber-head hammer and the total elongation of a surface-mounted optical fiber along the length of the repair material is measured as a function of load position. When a debonding patch is present, the induced sudden slope or sign change on the plot of fiber integral strain v. s. load position will reveal the extent and the location of the debonded area. The results of the study indicate that the proposed technique is applicable for debonding patch detection in repaired members under various support conditions.

Key words: fiber-reinforced plastic(FRP); bonded repair; debonding patch; fiber-optic interferometer; nondestructive testing

CLC number: TB330.1 **Document code**: A **Article ID**: 1005-1120(2017)03-0255-10

0 Introduction

Over the past decade, repair with fiber-reinforced plastic (FRP) plate, simple and effective, has become popular and been performed on various structures built with metal[1], polymeric composites and concrete[2,3]. Compared to steel, fiber-reinforced plastic plates offer higher strength/weight and improved durability. For the repair should be effective, the bonded plate must work together with the original structure[3]. However, under various conditions, interfacial debonding of the bonded plate from the substrate may occur[4]. Debonding may initiate at the end of the bonded plate, where a high strain gradient exists[5-7]. When the workmanship is not good enough, imperfect bonding may lead to the formation of debonded zones under the plate. Debonding may also result from moderate impact on the plate[8,9]. For those composite plates on concrete substrate, debonding may initiate at the bottom of a flexural crack, leading to the formation of a debonded region away from the edge of the plate[5-8]. Moreover, since the debonding is often in the form of a patch rather than a through-width crack, its effect on the adjacent stress period is inherently three-dimensional in nature. If debonding patch is left unnoticed, its continual growth will lead to the failure of the repair. The detection of the interfacial debonding patch in its early stage is hence a very important task in monitoring the "health" of structures retrofitted with bonded plates.

The traditional non-destructive methods for interface defects or debonding detection of FRP-strengthening components includes ultrasonic[10], X-ray[11], acoustic-emission[12], and infrared detection[13]. However, these methods have many shortcomings such as poor accuracy, low efficien-

* Corresponding author, E-mail: cexyx@hotmail.com.

How to cite this article: Xu Ying, Wang Dexiang, Tang Tianyou, et al. Debonding patch detection in FRP-strengthened materials with fiber-optic interferometer[J]. Trans. Nanjing Univ. Aero. Astro., 2017,34(3):255-264.
http://dx.doi.org/10.16356/j.1005-1120.2017.03.255

cy or harmful to human body. Since the late 1980s, optical fiber sensors have been utilized to detect delaminations inside FRP materials[14]. Interferometric type fiber optic sensors have advantages of high sensitivity and potentially high resolution compared with intensity type sensors. Therefore, they can be used for the damage detection in structural members. Xu Ying, et al. [15-18] have used a fiber-optic interferometer for delamination detection within composite material beams, which successfully assessed the delamination's existence, location and extent. The accuracy and practicability of the method was verified through both theoretical analysis and experimentally work.

We use a rubber-head hammer to apply loads point by point on the surface of a FRP strengthened plate along predetermined positions. It measures the integral strain on the surface of FRP sheets (namely, the total deformation of FRP sheets under loads along its length, which is the same as the integral strain of optical fiber) by attaching a sensor arm of a fiber-optic interferometer on the surface of the FRP sheet along the beam length. Then, through data processing, a relation curve of the loading location and the integral strain of the optical fiber is concluded. Due to the local influence of the debonded area on FRP sheet, the integral strain loaded on the debonded area and bonded area mutates. The existence and location of debonding patch of the bonded material can be observed from a sudden "jump" in magnitude of the integral strain v. s. load position curve. The purpose is to study the sensitivity of this method for detecting the delamination patches. This method has achieved good results in detecting debonded patches of FRP-strengthened concrete structures and FRP-strengthened aluminum alloy structures, thereby proving a useful method for debonding patch detection of FRP bonded materials.

1 Sensing Principle

The debonding sensing principle is illustrated in Fig. 1, which shows a beam member under arbitrary support conditions and an all-fiber Mach-Zehnder interferometer[19]. The carbon fiber sheets are bonded to the surface of the member as repair material. Part of the surface between repair material and substrate is assumed to have debonded. A load is applied at different positions along the upper surface of the repaired material. As Fig. 1 shows an instrumented hammer is employed as the loading device. However, the load can also be applied with other means. An optical fiber, which represents one arm of a fiber interferometer, is surface-mounted to the repaired material. The other arm is left free from loading.

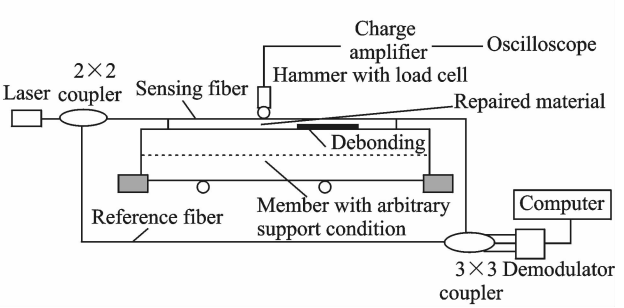

Fig. 1 Schematic of Mach-Zehnder interferometer

When the repaired material is under loading, the output of the interferometer is the optical phase shift that is proportional to the integral strain along the surface-mounted fiber. When part of the repair material has debonded the integral strain is different from that for the case with perfect bond. The difference depends on the extent of the debonding patch as well as the relative position of the debonding patch and the load. If they are far apart, the change may not be noticeable. When the load gets close to the debonding patch, a significant difference can be expected. Therefore, if a load is moved along the member, and the integral strain plotted as a function of load position, one should be able to identify both the debonding patch location and size.

In this paper, only surface-mounted fibers are considered. As a reasonable approximation, one can assume: ① Negligible disturbance of strain field by the surface-mounted optical fiber and ② perfect strain transfer from the matrix to optical fiber. Under such a situation, the optical

phase shift, ($\Delta\varphi$), measured from the fiber interferometer, is related to the integral strain along the fiber through[20]

$$\Delta\varphi=\frac{2\pi n}{\lambda}\left(1-\frac{n^2}{2}\left[P_{12}-\mu_f(P_{11}+P_{12})\right]\right)\left(\int_0^L\varepsilon_z\mathrm{d}s\right) \tag{1}$$

where n is the refractive index of the core, λ the optical wavelength, μ_f the Poisson's ratio and P_{ij} the Pockel's constants. Since the terms in front of the integral sign in Eq. (1) are constants for any given optical fiber system, the total phase shift ($\Delta\varphi$) is proportional to the integral strain ($\int\varepsilon_z\mathrm{d}s$). Therefore, from the measured phase shift, the integral strain can be easily calculated.

2 Principle of Signal Demodulation

In this paper, a 3×3 coupler is utilized for signal demodulation of the fiber optic interferometric sensors. The schematic diagram of a Mach-Zehnder interferometer terminated with a 3×3 coupler is shown in Fig. 2. It consists of a 2×2 coupler at the input and a 3×3 coupler at the output. The excitation is applied to the sensing arm of the interferometer. In an ideal 3×3 coupler, where there is an equal amount of light splitting into each arm, the outputs have the same magnitude and a relative phase difference of 120°. Mathematically, the outputs of the interferometer, i. e., the measured light intensities, can be expressed as

$$f_n(t)=C+B\cos\left[\varphi(t)-(n-1)\frac{2}{3}\pi\right] \tag{2}$$

where n is a labeling index which has values 1, 2 or 3, $\varphi(t)$ the phase modulation between the legs of the interferometer, and C a central value around which the output will vary with amplitude B.

Our objective is to measure the phase change $\varphi(t)$. In Eq. (2), C, B and $\varphi(t)$ are all unknowns. By measuring all the three outputs $f_1(t)$, $f_2(t)$ and $f_3(t)$ from the coupler, three equations are available at each time t for the three unknowns, specifically for $\varphi(t)$. With this approach, a much higher resolution than conventional fringe counting can be obtained.

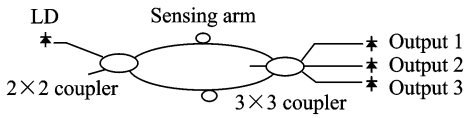

Fig. 2 Mach-Zehnder interferometer terminated with a 3×3 coupler

Besides high resolution over a large dynamic range, 3×3 coupler based demodulation also possesses good environmental stability and polarization insensitivity, and is thus very useful in practice. In earlier work with this technique, circuits are designed to perform the demodulation at real time. However, the error is often large. The use of commercially available software to perform the demodulation has been explained in Ref. [21]. By using this technique, not only complicated operating circuits are omitted, but also a high demodulating resolution is achieved. Moreover, by using software for demodulating operation, one can obtain the waveforms of intermediate steps and analyze the errors and their causes. In this investigation, the signals are also demodulated with the use of software.

3 Experiment

3.1 Materials for substrates

To demonstrate the feasibility of the technique, experimental testing of bonded repairs with interfacial debonding patches has been carried out on different substrates. CFRP sheets were used as repair material. Two common types of substrates, i. e. aluminum plates and concrete beams, were bonded with CFRP sheets using epoxy adhesive. These two types of substrates represent two loading configurations for CFRP bonded repair which will be explained in details in later part of this paper. The strength of concrete substrate is C30, and the geometry of it is 800 mm× 60 mm×60 mm. The surface of the concrete was polished with sandpaper. The geometry of the aluminum alloy substrate is 600 mm × 60 mm× 3 mm and the surface of the aluminum alloy was cleaned with Acetone.

3.2 Fabrication of debonding patches

Since the debonding patch only span across part of the plate′s width (Fig. 3(a)), it is difficult to make a specimen with a fully embedded debonding patch artificially. For simplification, we assume the location of the patch is symmetrical about the centerline of the width. Due to the symmetry of the patch about the centerline of the width direction, only half of the plate is taken into account (Fig. 3(b)). CFRP were made by hand lay-up of 4 plies of lamina (each ply with a thickness of 0.11 mm) along the same orientation, followed by curing under normal temperature. During the lay-up, the edge of each sheet has to be carefully aligned and epoxy is uniformly brushed onto the sheet. Pressure is applied through a small roller to avoid the formation of resin-rich regions or air bubbles. To introduce artificial debonding patches, a thin Teflon sheet (0.1 mm thickness) of specified width was placed at the interface between FRP and substrate. Releasing oil was applied on the surfaces of the sheet. After the composite laminate hardens, the sheet was pulled out from the side to introduce a debonding patch of known location and size. To simulate common cases of debonding in plate repair, the interfacial debonding patch was located either in the middle or at the edge of the CFRP laminates. The debonding patch size is 40 mm × 20 mm × 0.5 mm. Note that the 0.5 mm thickness of CFRP is within the range of bonded plates used in practice.

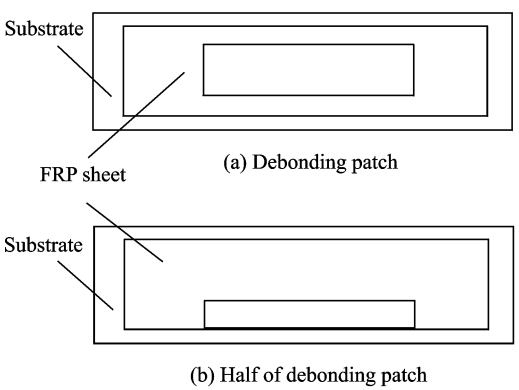

Fig. 3 Schemes of debonding patch and half of debonding patch

3.3 Experimental set-up

Two loading configurations were considered in this paper. The set-up for testing CFRP on simply supported substrates (i. e. alumimum plates) is shown schematically in Fig. 4, where C_p means the coading position. Mechanical rollers that allowed free rotation and axial sliding were used as supports at both ends. In Fig. 4, the debonding patch is shown in the middle of the plate, but tests with the debonding patch at the edge have also been performed. When CFRP is used to repair concrete members, due to the high strength of CFRP, only a very thin layer (less than 0.5% of the concrete member thickness) is required. Due to the significantly higher stiffness of the concrete member over the CFRP plate, the plate can be considered resting on a foundation made of concrete. The actual support condition on the other side of the concrete is not relevant. In the experiment, we have simply bonded the CFRP on one side of the concrete member, and support the other side on a flat surface. The loading configuration is schematically shown in Fig. 5, where concrete member is uniformly supported at its bottom.

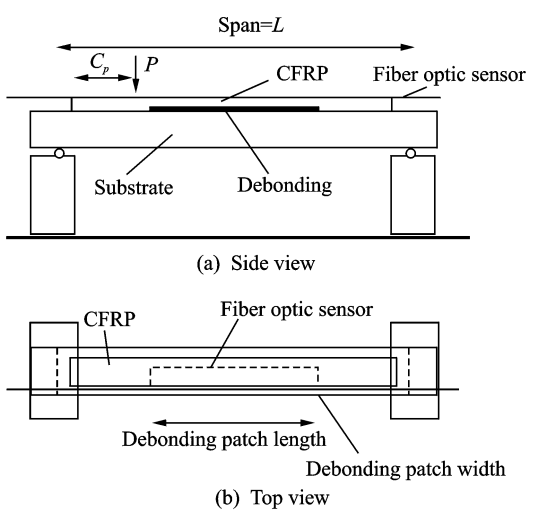

Fig. 4 Debonded CFRP on simply supported substrate and surface mounted optical fiber sensor

Differ from previous work which focused on "through" delaminations or debonding, debonding patches with optic fiber attached on the surface of the plate were made in the laboratory and the in-

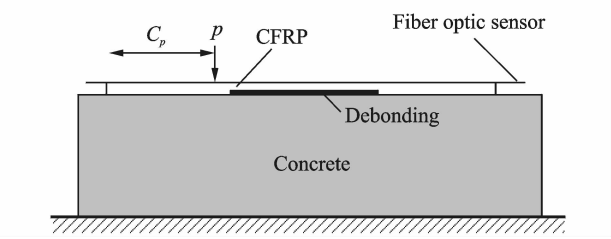

Fig. 5 Debonded CFRP elastically supported by concrete member and surface mounted optical fiber sensor

tegral strain along the optic fiber were measured with interferometry. The attachment location for the optical fiber and the loading location in this experiment are shown in Fig. 6. B is the width of delamination patch. Here, the 0 mm line, $B/2$ line, B line, and 10 mm line are utilized as both the attachment locations of the sensor arm of the interferometer and the load applying lines. Note that the 10 mm line fiber was located away from delaminated area along the width direction of the plate.

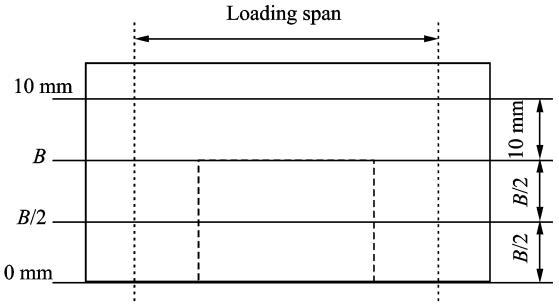

Fig. 6 Locations for optical-fiber attachment lines and loading lines

To measure strain on the repair material, the optical fibers was bonded properly to the upper surface of the CFRP laminates. The length change of the optical fiber was obtained with the Mach-Zehnder interferometric system. The sample frequency was 2 kHz. With the system, a displacement resolution of 1 nm under a dynamic loading could be achieved.

Due to the high sensitivity of interferometric measurement, the result was strongly affected by environmental noise due to air currents, vibrations and temperature fluctuations. In order to improve the signal/noise ratio, a quasi-impulse loading is applied. Since the impulse lasted for only a fraction of a second, the variation of interferometer noise over the load application period was very small. By properly removing the noise from the effect of the impulse, the integral strain could be reliably obtained. Load application with the hammer was very convenient, and the subsequent data analysis was simple. The method was hence applicable to practical inspection of large members.

To apply a quasi-impulse loading, an instrumented impact hammer with a rubber head was employed. With the rubber head, sufficient damping was provided to prevent excessive vibration of the specimen during the test. The hammer was connected to a charge amplifier and the force versus time was recorded by a 60 MHz digital storage oscilloscope (Tektronix 2212).

In the test, quasi-impulse loading was applied along the CFRP laminates at discrete points that were 10 mm apart. Actually, the closer the subsequent load positions are, the higher the "resolution" of the integrated strain v. s. position curve will be, and the easier the debonding is detected. Therefore, a small distance between adjacent loading points is desirable. From our experience, it appears the distance of 10 mm is a good compromise between testing efficiency and data resolution.

During the experimental process, the rubber-head hammer was used to apply loads point by point on the specified lines (Fig. 6) to cause a slight deformation of the FRP sheets. The integral strain obtained from interferometric measurement is then normalized by the peak force value, and plotted as a function of load position. The trend of the resulting curve is expected to be sensitive to the presence of debonding. Test results and their interpretations will be considered in the next section.

4 Results and Discussion

4.1 Feasibility of detection for debonding patch of FRP-strengthened concrete beam structure

To study the feasibility of this method in debonding patch detection under continuous sup-

port, FRP-reinforced concrete beams with 40 mm×20 mm debonding patch is utilized. The locations of the fiber line and the load line were used as two independent variables to analyze the influence of these two factors on detection feasibility. Fig. 7 shows raw data of normalized integral strain v. s. loading position curves when the load line was fixed in the 0 mm line and the fiber was attached on the 0 mm line, 10 mm line, and $B/2$ line, respectively. Note that In each figure the line segment denoted by L shows the actual extent of the interfacial debonding patch. Fig. 8 shows normalized integral strain v. s. loading position curves when the fiber position was fixed on the 0 mm line and the load line was located on the 0 mm line, 10 mm line, and $B/2$ line or B line, respectively. For each load position, the test was repeated three times, and the integral strain was obtained as the average value of the three results. The average variation of the testing result is about7% and the repeatability of the test method is therefore considered satisfactory. In this paper, the error tolerance between the detected debonding size and the actual debonding size is within 10 mm, which is equal to the interval between two adjacent loading points.

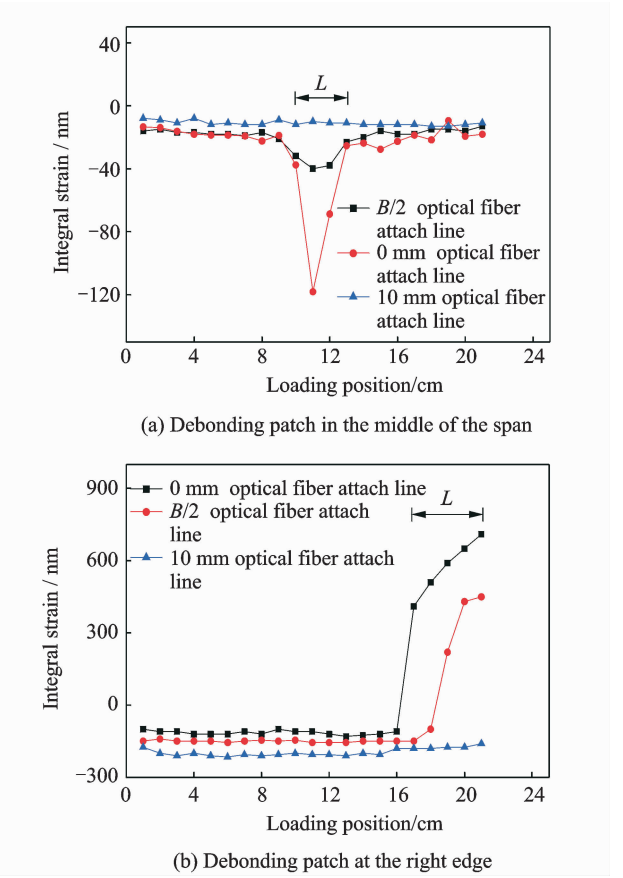

Fig. 7 Normalized integral strain vs. loading position curves for FRP on concrete member when loading at 0 mm line and optical fiber at different lines

Figs. 7, 8 show the results for debonded CFRP that is elastically supported by concrete substrate. The interfacial debonding was introduced in the middle of CFRP for Fig. 7(a) and Fig. 8(a) and at the edge of CFRP for Fig. 7(b) and Fig. 8(b). The results from the two figures show that when both the loading line (0 mm line and $B/2$ line or B line) and fiber line (0 mm line and B/2 line) pass the debonding patch, the integral strain almost keeps a constant when loading positions are away from debonding patch. However, once the debonding patch reaches the region within the line segment denoted by L in the figures, there is a sudden "jump" in magnitude of the integral strain, due to increasing slope (or more precisely, the increase in absolute value of the slope) of the integral strain v. s. loading position curve. We believe the constant value in integral strain from the support to the edge of the debonding is the global effect on a surface-mounted fiber that is under the continuous supported condition, while the part within the "jump" is resulted from local effects caused by the debonding. To support this argument, numerical analysis published previously[15] was referred for CFRP bonded perfectly on an elastic foundation and the results show that the integral strain value is very small under point-by-point loading and is nearly constant. Therefore, the integral strain curve for CFRP on an elastic foundation is a smooth flat line (except at two ends)[15]. By comparing experimental data in Figs. 7, 8 to smooth flat line, the extent and the location of the debonding can be identified from the region where the integral strain suddenly increases to a significantly higher magnitude.

However, when the load line passes the debonding patch but fiber line (at 10 mm line) does not pass the debonding patch (Fig. 7) or

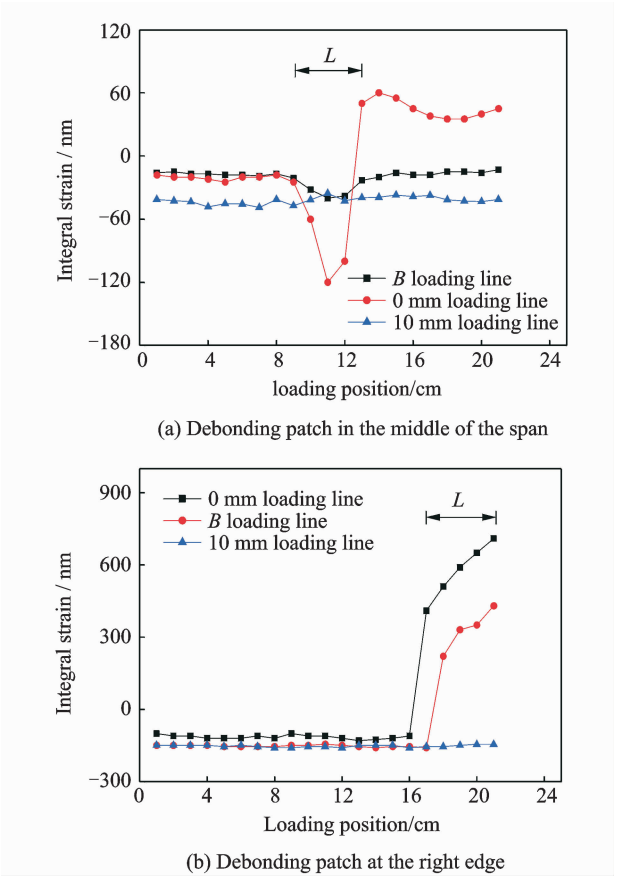

Fig. 8 Normalized integral strains v. s. loading position curves for FRP on concrete member when optical fiber at 0 mm line and loading at different lines

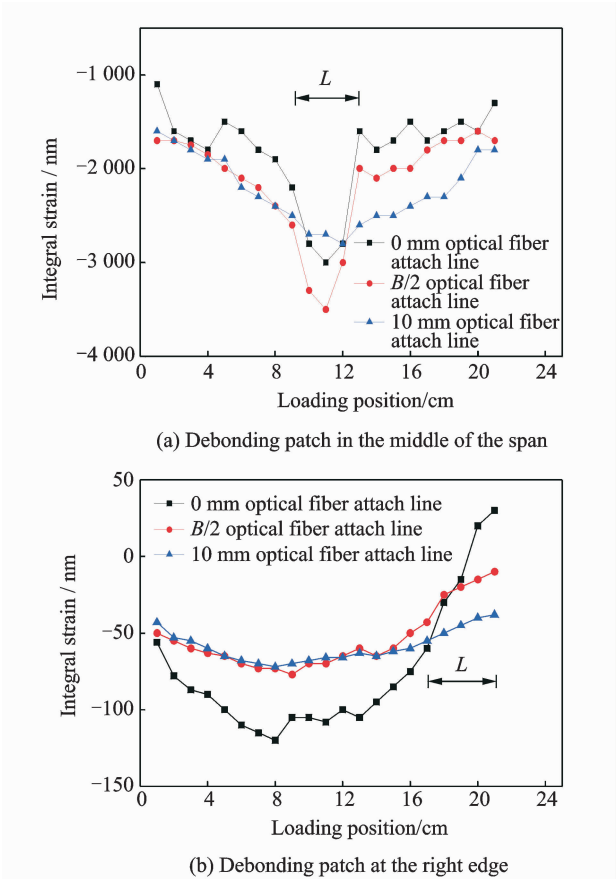

Fig. 9 Normalized integral strains v. s. loading position curves for FRP on simply supported aluminum plate when loading at 0 mm line and optical fiber at different lines

when the fiber line passes the debonding patch but the load line does not pass the debonding patch (load line at 10 mm line) (Fig. 8), regardless of the position of the debonding patch, the normalized integral strain v. s. loading position curve is always a flat line without sudden increase of values, and thus it is unable to identify the location and the size of the debonding patch precisely.

4.2 Measurment of structure of FRP-reinforced beams with aluminum alloy plates

Figs. 9, 10 show the results for debonded CFRP that is simply supported by aluminum alloy substrate. The interfacial debonding was introduced in the middle of CFRP for Fig. 9 (a) and Fig. 10 (a) and at the edge of CFRP for Fig. 9(b) and Fig. 10(b). The results from Fig. 9 (a) and Fig. 10 (a) show that when both the loading line (0 mm line and $B/2$ line or B line) and fiber line (0 mm line and $B/2$ line) pass the debonding patch, as shown in Figs. 9, 10 where the debonding patch is in the middle of the CFRP laminates, the integral strain increases with the distance increasing from the support. However, once the debonding is reached, there is a sudden "jump" in magnitude of the integral strain, due to increasing slope (or more precisely, the increase in absolute value of the slope) of the integral strain v. s. load position curve. We believe the increase in integral strain from the support to the edge of the debonding is the global bending effect on a surface-mounted fiber that is on the compression side under the simply supported condition, while the part within the "jump" is resulted from local effects caused by the debonding patch[14]. To support this argument, numerical analysis published in previous paper[15] was referred for the integral strain along a surface-mounted fiber for a perfect-

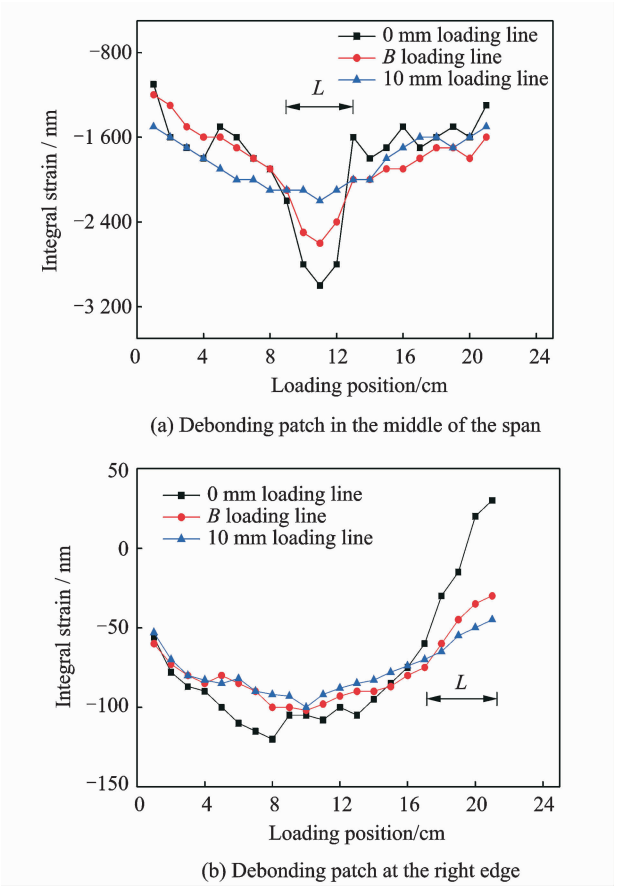

Fig. 10 Normalized integral strains v. s. loading position curves for FRP on simply supported aluminum plate when optical fiber at 0 mm line and loading at different lines

ly bonded repair member based on elementary beam bending theory[15]. The global response was represented by a quadratic curve. By comparing experimental data in Fig. 9(a) and Fig. 10(a) to quadratic curve, it appears that the location and the extent of the debonding can be deduced from the points where the slope of the integral strain v. s. loading position curve shows a sudden change.

For debonding patch at the edge of the CFRP laminates on simply supported substrate, the quasi-impulse loading was applied very lightly onto the surface of CFRP in order to minimize the global bending effect on the fiber. The results are shown in Fig. 9 (b) and Fig. 10(b). They show that the extent of debonded region can be obtained from an interesting observation about the sign of integral strain. Once the loading gets into the debonded region, the sign of the integral strain from the test tends to change from negative to positive. The change of the sign means the fiber is first under compression when the loading is outside the debonding patch zone and then under tension when the loading is on the top of the debonding patch zone. It is reasonable because when the loading is outside the debonding patch zone, the fiber is at the compression side of the whole structure. However, when the loading is on the top of the debonding patch, the debonded part acts like a cantilever under point loading and the fiber is under tension rather than compression. The sign change occurs over a small distance as the load point move through the internal boundary of the debonded region. From the sign change of the integral strain, the extent of the debonding zone can be identified.

However, when the load line passes the debonding patch but fiber line (at 10 mm line) does not pass the debonding patch (Fig. 9) or when the fiber line passes the debonding patch but the load line does not pass the debonding patch (load line at 10 mm line) (Fig. 10), regardless of the position of the debonding patch, the normalized integral strain v. s. loading position curve is approximately a quadratic curve without sudden increase of values or sign change, and thus it is unable to identify the location and size of the debonding patch precisely.

In addition, from Figs. 9, 10, one can tell that the normalized integral strain curve for debonded CFRP that is simply supported by aluminum alloy substrate is approximately a quadratic curve[15] and its value is much larger than that of the debonded CFRP that is continuously supported by concrete substrate. (Figs. 7, 8). Due to the influence from the overall deformation, the sudden increase of the integral strain value when the loading reaches the debonding patch is not so obvious as when it is under continuous support.

Before closing, an important practical aspect of the proposed debonding detection technique should be pointed out. From the results in this paper, the technique is able to identify the pres-

ence of debonding patch and provide an estimate of its size. However, due to the presence of fluctuations along the experimental curve, the exact location of the debonding region is difficult to obtain. Since the technique only involves a very simple testing procedure, and data interpretation is straight-forward, it can be employed in the structural inspection program as a very efficient first test to approximately locate the debonding patch zone. Detailed characterization of the debonding patch can then be carried out with more sophisticated and costly techniques.

5 Conclusions

Interfacial debonding patch between repair material and substrate is an important issue in bonded repair. In this paper, a new technique for debonding detection is presented. With loading applied at different positions, the integral strain (or total elongation) along the upper surface of the repair is measured with fiber optic interferometry. The debonding patch extent and location are then deduced from the integral strain v. s. loading position curve. To demonstrate the technique, experiments are carried out on aluminium and concrete members repaired with CFRP laminated plates. Based on the results, several guidelines for debonding patch detection can be proposed:

(1) For plate bonded on a stiff substrate that acts like an elastic foundation, debonding patch can be identified from the region where the integral strain suddenly increases to a significantly higher magnitude.

(2) For plate bonded on relatively thin substrates that act as beam members, debonding at the middle of the bonded plate can be observed from a sudden "jump" in magnitude of the integral strain, while debonding at the edge of the plate is reflected by a sudden change of the sign of the integral strain v. s. loading position curve.

(3) When this method is applied for debonding patch detection, only when the fiber line and load line are as close as possible to the debonding patch can the location and size of the debonding be accurately determined.

(4) The feasibility of debonding patch detection based on this method is found to be higher for FRP-strengthened structures under continuous support than under simple support.

Since the proposed debonding patch detection technique is very simple in execution and its data interpretation is straightforward, it should have high potential as a method for in-situ damage detection while in service.

Acknowledgment

This work was supported by the National Natural Science Foundation of China (No. 51278156) and the Basic Project of Shenzhen Science & Technology Program (No. JCYJ2017030155815876).

References:

[1] SEN R, LIBY L, MULLINS C. Strengthening steel bridge sections using CFRP laminates[J]. Composites, Part B: Engineering, 2001, 32(4):309-322.

[2] GUDONIS E, TIMINSKAS E, GRIBNIAK V, et al. FRP reinforcement for concrete structures: state-of-the-art review of application and design [J]. Engineering Structures & Technologies, 2013, 5(4): 147-158.

[3] TENG Jingguang, CHEN Jianfei, SMITH S T, et al. FRP reinforced concrete in structure [M]. Beijing: China architecture &building press, 2005. (in Chinese)

[4] QIAO P, DAVALOS J F. 17-design of all-composite structures using fiber-reinforced polymer(FRP) composites[J]. Developments in Fiber-Reinforced Polymer(FRP) Composites for Civil Engineering, 2013, 14(4): 469-508.

[5] HALLONET A, MICHEL L, FERRIER E. Investigation of the bond behavior of flax FRP strengthened RC structures through double lap shear testing[J]. Composites Part B Engineering, 2016, 100(2):247-256.

[6] SMITH S T, ZHANG H, WANG Z. Influence of FRP anchors on the strength and ductility of FRP-strengthened RC slabs [J]. Construction & Building Materials, 2013, 49(6):998-1012.

[7] LóPEZ-GONZáLEZ J C, FERNáNDEZ-GóMEZ J, DíAZ-HEREDIA E, et al. IC debonding failure in RC beams strengthened with FRP: Strain-based versus stress increment-based models [J]. Engineering Structures, 2016, 118: 108-24.

[8] OLLER E, MARí A R. Long-term bond stresses and debonding failure of FRP-strengthened RC cracked members [J]. Composites Part B Engineering, 2013, 52(9):30-9.

[9] JIANG X, KOLSTEIN M H, BIJLAARD F S K. Experimental and numerical study on mechanical behavior of an adhesively-bonded joint of FRP - steel composite bridge under shear loading [J]. Composite Structures, 2014, 108(1): 387-99.

[10] LANGENBERG KJ, MARKLEIN R, MAYER K. Ultrasonic nondestructive testing of materials [J]. Crc Press, 2012, 12(2): 34-39.

[11] ZHANG H J, ZHOU C W. Three-dimensional reconstructed finite element model for C/C composites by Micro-CT[J]. Transactions of Nanjing University of Aeronautics and Astronautics, 2015, 32(6):639-645.

[12] CHEN Z, LI D, LI Y, FENG Q. Damage analysis of FRP/steel composite plates using acoustic emission [J]. Pacific Science Review, 2015, 38(3): 193-200.

[13] TASHAN J, AL-MAHAIDI R. Bond defect detection using PTT IRT in concrete structures strengthened with different CFRP systems [J]. Composite Structures, 2014, 111(11): 13-19.

[14] SHEN Linghui, ZHAO Zhimin, YU Xiaolei. Design of remote monitoring internet of things system for new optical fiber smart structure [J]. Journal of Nanjing University of Aeronautics & Astronautics, 2015, 47(3):453-458. (in Chinese)

[15] XU Y, LEUNG C K Y, YANG Z, et al. A new fiber optic based method for delamination detection in composites [J]. Structural Health Monitoring, 2003, (3): 205-223.

[16] XU Ying, LEUNG C K Y, JIANG Ying. Delamination detection at web/flange junction of I-section GFRP beam with fiber optical interferometer sensor [J]. Fuhe Cailiao Xuebao/acta Materiae Compositae Sinica, 2007, 24(2): 143-150. (in Chinese)

[17] XU Y, LI Y Q, JIANG Y, et al. Application of 3× 3 coupler based Mach-Zehnder interferometer in delamination patch detection in composite[J]. Ndt & E International,2011, 44(5): 469-476.

[18] JIANG Ying, XU Ying, LEUNG C K Y. Embedded fiber optical Mach-Zehnder interferometer for the detection of delamination in composites [J]. Acta Materiae Compositae Sinica, 2004, 21(1): 129-133. (in Chinese)

[19] XU Y. Delamination detection at web/flange junction of I-section composite beam with fiber optical interferometer sensor [J]. Composites Part B Engineering, 2014, 58(3): 140-146.

[20] HER S C, YANG C M. Dynamic strain measured by Mach-Zehnder interferometric optical fiber sensors [J]. Sensors, 2012, 12(3): 3314-26.

[21] XU H, QIAO Z. A novel demodulation method for fiber optic interferometer sensor using 3 × 3 coupler [M]. Springer International Publishing, 2014, 967-975.

Dr. **Xu Ying**, an associate professor, received B. S degree in civil engineering from Dalian University of Technology in 1999 and Ph. D. degree in building materials professional from Hong Kong University of Science and Technology in 2004, respectively. From Jan., 2005 to Mar., 2005, she worked as a visiting scholar in Department of Civil Engineering of Hong Kong University Science & Technology. From Apr., 2005 to Aug., 2007, she worked as a research and development engineer in Shenzhen Institute of Building Research. From Sep., 2007 to present, she has been worked in School of Civil and Environmental Engineering, Shenzhen Graduate School, Harbin Institute of Technology where she is currently a full associate professor. Her research is focused on FRP application in civil engineering, civil engineering structural health monitoring, fiber optic sensor, new structure and new material structure.

Mr. **Wang Dexiang** received the Master's degree in civil engineering from Harbin Institute of Technology, China, in 2012. His research is focused on debonding patch detection in FRP-strengthened materials and relevant fields.

Mr. **Tang Tianyou** received the B. S. degree in civil engineering from China University of Mining and Technology in 2015, and he enrolled in Harbin Institute of Technology in September, 2015. His research is focused on structural health monitoring, recycled aggregate concrete and relevant fields.

Ms. **Lu Miaomiao** received the B. S. degree in civil engineering from Henan Polytechnic University in 2015, and she enrolled in Harbin Institute of Technology in September, 2015. Her research is focused on structural health monitoring, carbon fiber reinforced composite and relevant fields.

(Executive Editor: Zhang Bei)